Dynamics of an erbium-doped fiber laser

E. Lacot, F. Stoeckel, and M. Chenevier
Laboratoire de Spectrométrie Physique, Boîte Postale 87, Université Joseph Fourier, F-38402 Saint Martin d'Hères Cedex, France
(Received 23 November 1993)

The temporal dynamics of an erbium-doped fiber laser shows various interesting modes of behavior. In the stationary regime, a behavior going from a cw working mode to deterministic chaos through different self-pulsed working modes has been observed. In the transient regime, effects such as antiphase phenomena, between two orthogonal states of polarization, can be observed. To describe the dynamics of the fiber laser we have studied a theoretical model based on two coupled lasers coherently pumped. A linear stability analysis is given which demonstrates the existence of a Hopf bifurcation for low values of the pump parameter. Numerical calculation results allow a good description of the experimental results. The value of the newly introduced coherence lifetime parameter is discussed.

PACS number(s): 42.60.Mi, 42.55.Wd

I. INTRODUCTION

Although people have always tried to build continuous lasers as stable as possible since their discovery, for the last few years it has appeared that under some conditions continuous lasers, even when running monomode, could deliver an intensity that varies erratically with time. This behavior, which appeared to be paradoxical in quantum optics, was in fact well known in other fields such as hydrodynamics (Rayleigh-Bénard instability) or chemical kinetics (Belousov-Zhabotinsky reaction). In 1975 Haken [1] showed the similarity between the equations of a monomode laser and those of the Lorenz system of atmospheric turbulence. This observation shows that chaotic behavior is possible in lasers. This initiated much theoretical and experimental work to characterize laser instabilities [2–9].

The interest in studying such effects in lasers and more particularly in fiber lasers is due to the fact that they can be described by a limited number of degrees of freedom and have short characteristic times in the microsecond to millisecond range, permitting an easy way of studying temporal dynamics [10,11].

In addition to their interest in telecommunications, fiber lasers are also interesting systems for nonlinear dynamic studies. Indeed the high power densities present in the core of the fiber permit the observation of different dynamic behavior going from a continuous working mode to deterministic chaos via a self-pulsed working mode, beating and antiphase phenomena [12]. The presence of instabilities and of self-pulsed working mode in solid-state lasers has been observed as early as the first experiment on the ruby laser in 1960 [13]. The physical origin of these pulses continues however to be the subject of ongoing research [14–20].

The dynamics of an Er^{3+} doped fiber laser has been analyzed under continuous and modulated pumping. Under continuous pumping, by increasing the pump power, the erbium-doped fiber laser reaches a Hopf bifurcation leading the laser from a cw mode to a self-pulsed mode operation. We have also observed that, both in the continuous and in the pulsed working mode, the transient behavior of the total intensity of the fiber laser is in fact the sum of the transient behavior of two orthogonal states of polarization which present beating and antiphase phenomena. In response to a stepped pumping, the fiber laser exhibits relaxation oscillations. Using a sinusoidal modulation of the pump power near the relaxation frequency we have observed in the dynamic behavior of the laser a period-doubling cascade leading to chaos. To describe the dynamics of the fiber laser, we have developed a semiclassical model based on two coupled lasers coherently pumped.

This paper is organized as follows. In Sec. II, we will describe the experiment and briefly report the various observed types of dynamic behavior published elsewhere [10]. We will also give the physical parameter that can be determined from these observations. In Sec. III, we propose a model that describes the transition between the cw and the self-pulsed mode for a weak value of the pump parameter (of the order of 1.5 to 2) and the antiphase phenomena between the two orthogonal states of polarization. In Sec. IV, we will discuss the steady-state solutions, make a linear stability analysis, and give the conditions required for a Hopf bifurcation. In Sec. V, we will perform a numerical calculation of the equations for the transient and the stationary states. These numerical results are compared with the experiments, and the value of the newly introduced coherence lifetime parameter is discussed.

II. EXPERIMENTAL RESULTS

The experimental setup is shown schematically in Fig. 1. The active medium is an erbium-doped fiber with a length between 1 and 10 m, doped with 40 to 2000 ppm of Er^{3+}. The core diameter is 6.4 μm and the fiber is single mode at the laser operating wavelength (1.538 μm). The pump laser is a krypton ion laser, and the beam passes through an acousto-optic modulator (AOM) controlled by a function generator. The AOM is mainly used to study the transient behavior (stepped pumping mode).

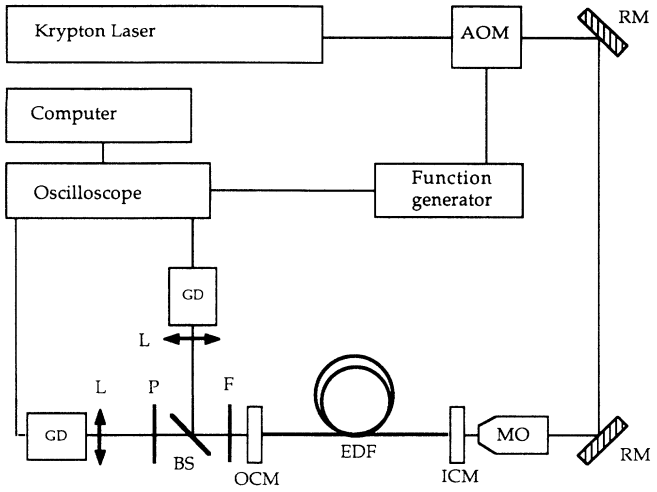

FIG. 1. Experimental setup of an erbium-doped fiber laser. AOM: acousto-optic modulator; RM: reflecting mirror; MO: microscope objective; ICM: input coupling mirror ($R_1 > 99\%$ at 1.538 μm); EDF: erbium-doped fiber; OCM: output coupling mirror ($R_2 = 40$–90% at 1.538 μm); F: high-pass filter ($\lambda > 850$ nm); BS: beam splitter; P: polarizer; L: lens; GD: germanium detector.

While in the cw pumping mode, the AOM is used as a variable attenuator. For this latter case the intensity of the first-order beam can then be changed without any angular deviation that would occur if the krypton laser power was monitored electrically. Such a procedure avoids, for example, false hysteresis in the characteristic curve of the fiber laser power arising from small angular deviation combined with thermal effects. The pump wavelength is fixed at 647 nm, and the erbium-doped fiber is pumped longitudinally through a $\times 10$ microscope objective with a numerical aperture of 0.2 and through the input dichroic mirror which is transparent at the pump wavelength but has a reflection coefficient $R_1 > 99\%$ at the laser operating wavelength. The output mirror is also butt-coupled to the fiber and has a reflection coefficient R_2 between 0.4 and 0.9. After a high-pass filter blocking the residual krypton pump beam, a beam splitter is used to record the laser intensity either directly for the total intensity or through a polarizer adjustable in rotation for the detection of one of the two orthogonal directions of the polarization. In all cases, the laser intensities are recorded by germanium detectors.

In typical operating conditions, the threshold pump power is of the order of 100 mW at the fiber input, and the maximum pump power available is about 500 mW. The near infrared (1.538 μm) output power obtained at the fiber output is of the order of a few mW.

A. Fiber laser, cw pumped

We have investigated the dynamic behavior of the fiber laser in the case where the spectrum is centered around 1.538 μm. By using the low-finesse Fabry-Pérot effect resulting from the small distance between the fiber and the output mirror, it is possible to obtain simultaneously the laser emission on the two wavelengths corresponding to the first and the second peak of the gain curve [10]. In this latter case, the laser emission presents a more complex dynamic behavior which is not the subject of this study.

For a pump power lower than the threshold pump power, $P < P_{th}$, the infrared intensity detected corresponding to the spontaneous emission is small and can be neglected ($I \approx 0$). When $P = P_{th}$ the laser reaches a stability exchange bifurcation, the solution $I = 0$ becomes unstable and the laser reaches a continuous working mode. For a pump power between P_{th} and a given pump power P_H ($P_{th} < P < P_H$), this solution is stable, and the laser intensity increases linearly with the pump power. When $P = P_H$ the laser reaches a Hopf bifurcation, the cw steady state becomes unstable and the total intensity of the fiber laser exhibits a self-pulsed working mode. Under our conditions, for $P > P_H$ this last solution always remains stable and the shape of the pulses changes from a near sinusoidal function to a narrower and deeper function when the pump increases. For much higher pump power, not experimentally reached here, it is possible that the laser could exhibit more complex pulsed behavior showing for example a period-doubling phenomenon. Figure 2 shows the response of the fiber laser in response to stepped pumping for two different pumping conditions. In the first case $P_{th} < P < P_H$ [Fig. 2(a)], after transient relaxation oscillations the fiber laser reaches in the stationary state a continuous working mode. In the second case $P > P_H$ [Fig. 2(b)], after transient relaxation oscillations the fiber laser reaches in the stationary state a self-pulsed working mode. Under our typical operating

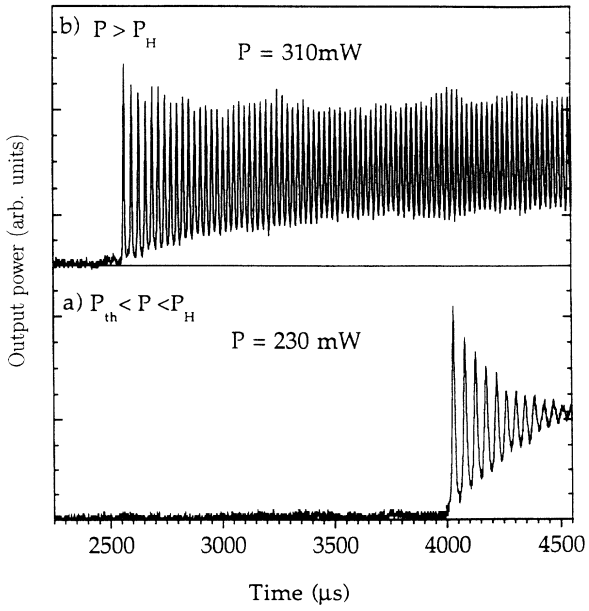

FIG. 2. Experimental transient behavior of the fiber laser in response to a stepped pumping ($t = 0$) for two values of the pump power: (a) $P_{th} < P < P_H$, the steady state is a continuous working mode; (b) $P > P_H$, the steady state is a self-pulsed working mode.

conditions, the frequency of the pulses is an increasing function of the pump power and varies between about 10 and 50 kHz when the pump power at the fiber input changes from 100 to 500 mW.

From these experimental results, the measurement of the buildup time and of the frequencies of the relaxation oscillations of the fiber laser versus the pump power allows us to determine the laser parameters [10]: the lifetime T of the photon in the cavity ($T \approx 10$ ns), the lifetime T_1 of the population inversion ($T_1 \approx 100$ μs), and the variation range of the pump parameter α ($1 < \alpha < 3$). The pump parameter is defined as the ratio of the inversion population produced by the pump power used to the threshold inversion population. Under our typical operating conditions, the transition between the cw working mode and the self-pulsed working mode occurs for a value of the pump parameter of the order of 1.5.

As for the Nd^{3+} doped fiber laser [12], the response of the total intensity I_{tot} of the Er^{3+} doped fiber laser to a stepped pumping is the sum of the responses of the intensities I_1 and I_2 of two orthogonal states of polarization. For the pumping condition $P_{th} < P < P_H$, the results obtained experimentally are represented in Fig. 3, where the response of the intensity of the first (I_1) and of the second (I_2) states of polarization are given on the upper and the middle traces [Figs. 3(a) and 3(b)], while the time variation of the total intensity $I_{tot} = I_1 + I_2$ is given in the lower trace [Fig. 3(c)].

During the transient regime, each state of polarization is a superposition of two damped oscillations with two different oscillation frequencies (beating). The fast one ω_R corresponds to the relaxation oscillation frequency previously used to determine the laser parameters while the lower frequency ω_L is associated with a new relaxation mode that appears in the fiber due to a cross-saturation coupling between two modes representing the two orthogonal states of polarization [21–24]. The comparison of the results of Figs. 3(a) and 3(b) shows that the high-frequency oscillations (relaxation frequency) are in phase while the low-frequency oscillations are in opposite phase (antiphase phenomena [12]). As these latter oscillations have almost the same amplitude, they destructively interfere, and as a result the total intensity exhibits damped oscillations with only the high oscillation frequency [Fig. 3(c)]. This result indicates that the total intensity $I_1 + I_2$ is an eigenstate of the fiber system. The second eigenstate with the slow relaxation oscillations corresponds to the difference $I_1 - I_2$. It cannot be observed directly in this experiment, but the time variation of the two orthogonal states of polarization, which present beating and antiphase phenomena, is a proof of its existence. The results experimentally obtained for the pumping condition $P > P_H$ are represented in Fig. 4. As previously, the transient behavior of the total intensity of the fiber laser is also the sum of the transient behavior of two orthogonal polarized intensities, which present beatings and antiphase phenomena. In this case, however, only the slowest frequency is damped. This is why the total intensity exhibits, both in the transient and in the asymptotic regime, oscillations with only the high oscillation frequency.

B. Fiber laser with a periodic pump modulation—chaos

The experimental identification of deterministic chaos can be achieved by studying the way that the solutions

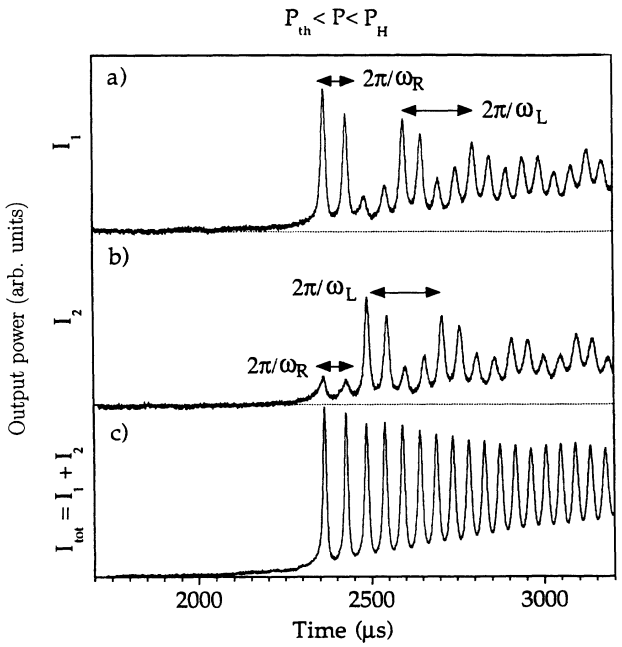

FIG. 3. Experimental transient behaviors of the intensities I_1 and I_2 of the two orthogonal states of polarization and of the total intensity I_{tot} in response to a stepped pumping ($t = 0$) when $P_{th} < P < P_H$.

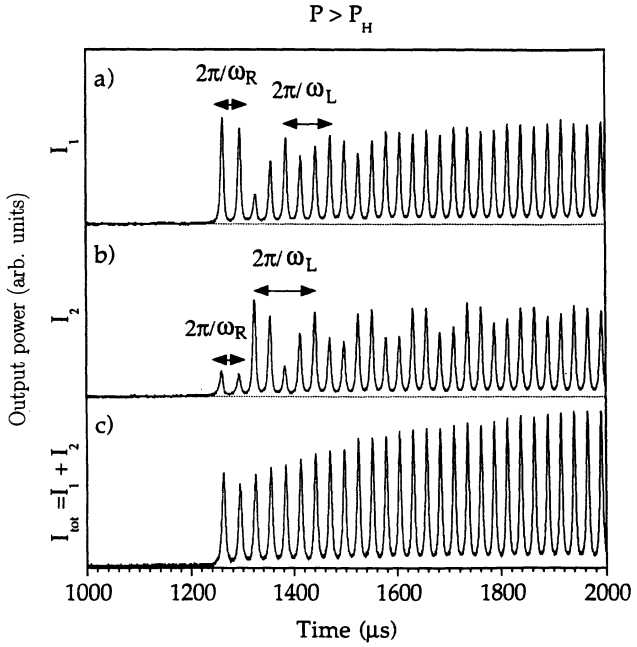

FIG. 4. Experimental transient behaviors of the intensities I_1 and I_2 of the two orthogonal states of polarization and of the total intensity I_{tot} in response to a stepped pumping ($t = 0$) when $P > P_H$.

take when they evolve from a stable solution to a chaotic state. Surprisingly it appears that for a system characterized by one control parameter, only a limited number of ways leading to chaos exists: the first one is the period-doubling cascade, the second is the intermittence, while the third is the appearance of incommensurable frequencies [25]. For more complex systems characterized by more than one control parameter, the chaos is approached by a combination of these three basic ways.

In lasers, chaos can appear either spontaneously, or when one control parameter is modulated, or when they are submitted to an injected signal [2]. It is by applying a sinusoidal modulation of the pump power near the relaxation frequencies (ω_R and ω_L) that we have been able to observe, in the dynamic response of the erbium-doped fiber, nonlinear phenomena and therefore more complex dynamic behavior. Figure 5 illustrates the evolution of such a nonlinear dynamic behavior for different values of the modulation frequency in the neighborhood of the highest relaxation frequency (ω_R) [10]. In our typical modulating conditions, the maximum pump power at the input of the fiber is 450 mW and the resonance frequency (ω_R) of the fiber laser is of the order of 45 kHz. Far from resonance [Fig. 5(a)] the laser response is linear, and a sinusoidal modulation of the pump power generates a laser intensity response at the same frequency. On the other hand, as soon as we approach the resonance frequency [Figs. 5(b) and 5(c)] the laser response becomes nonlinear, and the laser intensity is modulated with a double period ($2T$) and afterwards with a quadruple period ($4T$) of that of the pump power before losing all regularity and varying erratically with time [Fig. 5(d)].

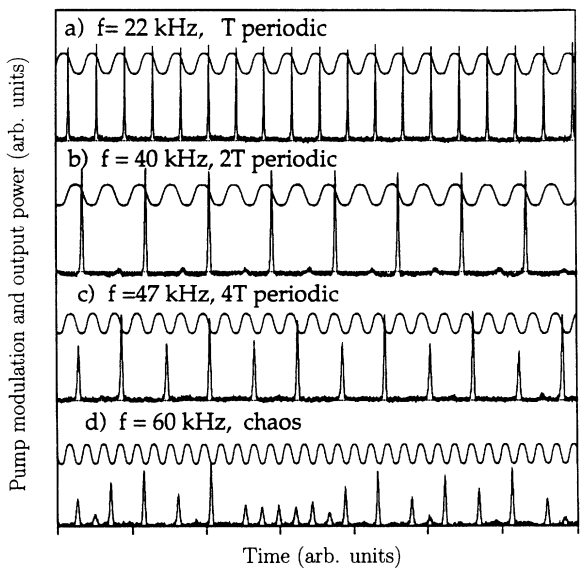

FIG. 5. Experimental time evolution of the total intensity of the fiber laser in response to a sinusoidal modulation of the pump power (upper trace) for different values of the modulation frequency (a) $f=22$ kHz, T-periodic response; (b) $f=40$ kHz, $2T$-periodic response; (c) $f=47$ kHz, $4T$-periodic response; (d) $f=60$ kHz, chaotic response. The time scale is different from one plot to another.

As mentioned above, the occurrence of an erratic regime after a succession of such period doubling is a proof that the fiber laser exhibits deterministic chaos.

III. MODELING OF THE FIBER LASER

In order to have a realistic model of the dynamics of the fiber laser the model must take into account the following points.

(i) The existence of a transition (Hopf bifurcation) between the cw and the self-pulsed working mode for a weak value of the pump parameter (of the order of 1.5 to 2).

(ii) The existence of beating and antiphase phenomena between two orthogonal polarization states of the emitted laser light.

(iii) The appearance of a period-doubling cascade leading to chaos in response to an external modulation of the pump power.

(iv) The experimentally determined laser parameters.

A. Modeling of the polarization effect

Despite the strongly multimode nature of the fiber laser due to a broad gain profile and the long cavity length, the experimentally observed behavior suggests that to a first approximation the fiber laser can be described as a two-mode laser in which each mode is associated with one of the orthogonal polarization eigenstates. Therefore, as in the Nd^{3+} doped fiber laser, we will not consider for the case of the Er^{3+} fiber laser the many longitudinal modes, but rather consider the laser as made of two subsets corresponding to two clusters of longitudinal modes, one in each state of polarization. Such a laser can be described by a phenomenological model of two class-B lasers coupled by their intensities and population inversions with the following set of equations [12]:

$$\begin{aligned}
\dot{I}_1 &= 2k[I_1(D_1+\beta D_2)-I_1] , \\
\dot{I}_2 &= 2k[I_2(D_2+\beta D_1)-I_2] , \\
\dot{D}_1 &= \gamma_{\parallel}[\alpha_1-D_1-D_1(I_1+\beta I_2)] , \\
\dot{D}_2 &= \gamma_{\parallel}[\alpha_2-D_2-D_2(I_2+\beta I_1)] ,
\end{aligned} \tag{1}$$

where I_1, D_1, I_2, and D_2 are, respectively, the reduced intensity and population inversion of the laser subsystems 1 and 2 associated with each state of polarization, and where $1/k$, $1/\gamma_{\parallel}$, and α are, respectively, the photon lifetime, the population inversion lifetime, and the pump parameter. The coupling parameter $\beta<1$ permits the description of the cross-saturation phenomena taking place inside the fiber and the interaction of each laser intensity with the population inversion of the other laser subsystem.

In our experimental setup the principal losses are due to the coupling between the fiber and the cavity mirrors. These losses are also isotropic, and in consequence the parameter k is the same for the intensities of the two coupled lasers. In the same manner, the value of the parameter $\gamma_{\parallel}$, which is a characteristic of the optical fiber, is isotropic and therefore is the same for the two orthogonal

states of polarization. On the other hand, the pumping parameters α_1 and α_2 of each population inversion are chosen to be different because the pump polarization changes the pump power distribution between the two orthogonal polarization eigenstates of the fiber.

This simple model allows a very good description of the experimentally observed transient behavior in Fig. 3 [10,26] and allows us to determine the strength of the coupling between the two orthogonal states of polarization. Indeed, a linear stability analysis of this simple model of two coupled class-B lasers shows that the square of the highest and the square of the lowest relaxation frequencies ω_R^2 and ω_L^2 vary linearly with the pump power and that their ratio depends only on the coupling parameter β and is given by

$$\frac{\omega_R^2}{\omega_L^2}=\frac{(1+\beta)^2}{(1-\beta)^2} . \tag{2}$$

From the experimental results of Fig. 6, which show the evolution of ω_R^2 and ω_L^2 versus the pump power, we determine an experimental value of $\beta=0.5$. This value indicates that in the fiber core a strong interaction takes place between the two orthogonal states of polarization.

We must also note that the beating and antiphase phenomena experimentally observed can also be interpreted in the frame of a multimode laser theory including spatial hole burning [21–24,27,28]. But in order to reduce the number of variables and adjustable parameters we prefer the use of the above-described phenomenological model of two class-B coupled lasers.

Although this model of two coupled class-B laser allows a good description of the experimentally observed transient behavior shown in Fig. 3, it is insufficient to describe all the fiber dynamics. Indeed the linear stability analysis shows that in this model any Hopf bifurcation occurs and therefore any self-pulsed working mode occurs. Nevertheless this model of two coupled lasers is a good base to start a fiber laser model.

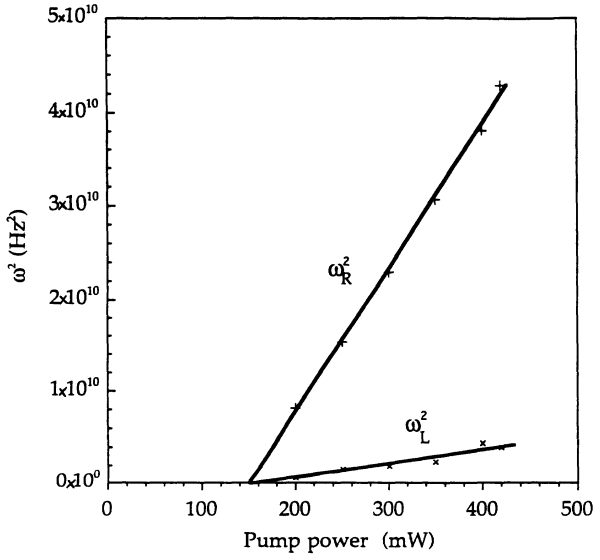

FIG. 6. Evolution of the squares of the highest and of the lowest frequencies of the relaxation oscillation ω_R^2 and ω_L^2 versus the pump power.

B. Modeling of the self-pulsed working mode

The appearance of spontaneous pulsation in the form of an undamped train of pulses in solid-state lasers was observed as early as 1960 during the first experiment on the ruby laser [1]. The physical origin of instabilities in such lasers continues, however, to be the subject of ongoing research [3].

The earliest stability analysis of the full set of semiclassical equations is due to Haken [29,30] and Risken [31] who showed that in the Maxwell-Bloch equation describing a homogeneously broadened single mode laser, there is a second threshold value above which no stable stationary solution exists. But this theory does permit the description of the cw mode as well as the self-pulsing one but is not sufficient to describe the dynamic behavior of the fiber laser. Indeed, a linear stability analysis shows in this case that the necessary conditions for the existence of a Hopf bifurcation are that the pumping level must be at least nine times above the threshold [in contradiction with above point (i)] and that the field decay rate exceeds the sum of the inversion, and the matter polarization decay rate $k>\gamma_\perp+\gamma_\parallel$. This latter condition, usually called the "bad cavity condition," is in contradiction with above point (iv) because for the fiber laser $\gamma_\perp \gg k > \gamma_\parallel$. Recently, an advance was made by Casperson [32], who showed that instabilities of the steady-state solution of the single-mode laser equations are much easier to realize in the case of inhomogeneous broadening. The Casperson instability requires a bad cavity condition but not the high pumping level needed for single-mode instability in the homogeneous case. In a further step Puccionni *et al.* [18] showed that the instability threshold for a laser operating in both states of polarization can be much lower than the Haken second threshold and does not require the bad cavity condition. Unfortunately, above the Hopf threshold this model does not describe well the experimental results [point (ii)] [26]. In 1987, Ryan and Lawandy [19] showed an instability threshold for an excitation 1.6 times above the first threshold in a three-level coherently pumped laser.

This last model, which gives a low threshold and exhibits a period-doubling sequence and chaos in agreement with point (i) and (iii), must be a good base to start the description of the fiber laser dynamics. In order to take into account points (ii) and (iv), we have coupled two such coherently pumped lasers in the same manner as in Sec. III A.

Before coupling the two lasers, let us consider only levels (1), (2), and (3) of our atomic system represented in Fig. 7. Such a three-level quantum system, where the transition $1\rightarrow 3$ is resonantly optically pumped by an electromagnetic field of magnitude E_P and where lasing of strength E_1 occurs from transition $2\rightarrow 1$, can be described by the following equations of the familiar density matrix elements ρ [29]:

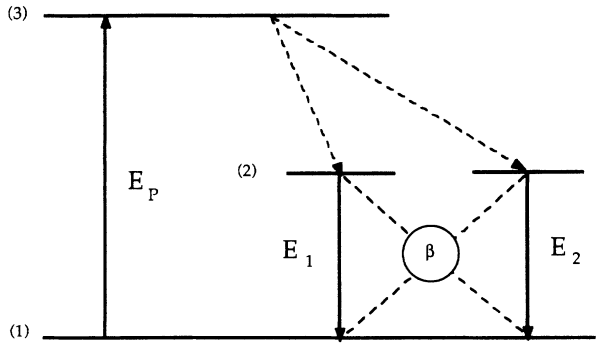

FIG. 7. Energy level diagram and fields in our model of two coupled lasers coherently pumped.

$$
\begin{aligned}
&\dot{\rho}_{21}=-\gamma_{\perp}\rho_{21}-i\omega_{21}\rho_{21}+iV_{21}(\rho_{22}-\rho_{11})+iV_{31}\rho_{32}^{*}\ ,\\
&\dot{\rho}_{31}=-\gamma_{\perp}\rho_{31}-i\omega_{31}\rho_{31}+iV_{31}(\rho_{33}-\rho_{11})+iV_{21}\rho_{32}\ ,\\
&\dot{\rho}_{32}=-\gamma_{c}\rho_{32}-i\omega_{32}\rho_{32}+i(V_{21}^{*}\rho_{31}-V_{31}\rho_{21}^{*})\ ,\\
&\dot{\rho}_{33}=i(V_{31}^{*}\rho_{31}-V_{31}\rho_{31}^{*})-A_{32}\rho_{33}\ ,\\
&\dot{\rho}_{22}=i(V_{21}^{*}\rho_{21}-V_{21}\rho_{21}^{*})+A_{32}\rho_{33}-A_{21}\rho_{22}\ ,\\
&\dot{\rho}_{11}=i(V_{31}\rho_{31}^{*}+V_{21}\rho_{21}^{*}-V_{31}^{*}\rho_{31}-V_{21}^{*}\rho_{21})+A_{21}\rho_{22}\ ,\\
&\rho_{11}+\rho_{22}+\rho_{33}=1\ ,
\end{aligned}
\tag{3}
$$

where A_{ij} is the spontaneous transition probability between the levels i and j, and where V_{31} and V_{21} could be expressed as a function of the complex electrical fields E and the dipole momentum μ_{ij},

$$
V_{31}=\frac{\mu_{31}E_{p}}{2h},\quad V_{21}=\frac{\mu_{21}E_{1}}{2h}\ . \tag{4}
$$

The coherence term ρ_{32} between the upper two levels (3) and (2) is induced by the mutual dipole interaction that these two levels have with the ground-state level (1), [19].

By defining the polarization of the medium and the population inversion densities in the usual manner, by using the rotating wave approximation, by neglecting the level-3 population with regard to the other levels's populations [25], and by using the Maxwell equations for the fields, a five-equation system can be obtained for the slowly varying amplitudes,

$$
\begin{aligned}
&\dot{E}_{1}=-kE_{1}-ig^{*}P_{1}\ ,\\
&\dot{P}_{1}=-\gamma_{\perp}P_{1}+igD_{1}E_{1}+igE_{P}C_{32}^{*}\ ,\\
&\dot{D}_{1}=-A_{21}(D_{1}+N_{\mathrm{tot}})\\
&\qquad+i[(2g^{*}E_{1}^{*}P_{1}-gE_{P}P_{P}^{*})-\mathrm{c.c.}]\ ,\\
&\dot{P}_{P}=-\gamma_{\perp}P_{P}+ig\frac{(D_{1}-N_{\mathrm{tot}})}{2}E_{P}+igE_{1}C_{32}\ ,\\
&\dot{C}_{32}=-\gamma_{c}C_{32}+i(g^{*}E_{1}P_{P}-gE_{P}P_{1}^{*})\ ,
\end{aligned}
\tag{5}
$$

in which E,P represent, respectively, the electrical field, the polarization of the medium and $k,\gamma_{\perp}$ their respective relaxation constants, while D and A_{21} represent, respectively, the population inversion and the spontaneous transition probability between the levels (1) and (2). The subscript p indicates the pump transition between the levels (1) and (3), while the subscript 1 is for the laser transition between the levels (2) and (1), γ_{c} is the relaxation constant relative to the newly introduced coherence term C_{32}, g is a coupling constant and N_{tot} is the total population of our atomic system. For the sake of simplicity, the coupling constant g and the matter polarization relaxation constant $\gamma_{\perp}$ are considered to be the same for the pump transition and the signal.

The system can be further simplified by supposing that the fields are initially in quadrature with their respective polarizations and by introducing the following normalized values [6]:

$$
\begin{aligned}
&E_{P}=\frac{\sqrt{\omega_{p}\gamma_{\perp}}}{g},\quad E_{1}=\frac{\sqrt{\omega_{p}\gamma_{\perp}}}{2g}\hat{E}_{1}\ ;\\
&P_{P}=\frac{ik\sqrt{\omega_{p}\gamma_{\perp}}}{2|g|^{2}}\hat{P}_{P},\quad P_{1}=\frac{ik\sqrt{\omega_{p}\gamma_{\perp}}}{2|g|^{2}}\hat{P}_{1}\ ;\\
&D_{1}=\frac{k\gamma_{\perp}}{|g|^{2}}\hat{D}_{1},\quad C_{32}=\frac{k\gamma_{\perp}}{|g|^{2}}\hat{C}_{32},\quad N_{\mathrm{tot}}=\frac{k\gamma_{\perp}}{|g|^{2}}\hat{N}_{\mathrm{tot}}\ ;
\end{aligned}
\tag{6}
$$

where ω_{p} is the absorption probability of a pump photon.

Dropping the $\hat{}$ sign, we obtain the following set of real equations for the slowly varying amplitude:

$$
\begin{aligned}
&\dot{E}_{1}=-k(E_{1}-P_{1})\ ,\\
&\dot{P}_{1}=-\gamma_{\perp}(P_{1}-D_{1}E_{1}-C_{32})\ ,\\
&\dot{D}_{1}=-A_{21}(D_{1}+N_{\mathrm{tot}})-\omega_{p}(P_{1}E_{1}+P_{p})\ ,\\
&\dot{P}_{p}=-\gamma_{\perp}[P_{p}-(D_{1}-N_{\mathrm{tot}})-E_{1}C_{32}]\ ,\\
&\dot{C}_{32}=-\gamma_{c}C_{32}-\frac{\omega_{p}}{4}(2P_{1}+E_{1}P_{P})\ .
\end{aligned}
\tag{7}
$$

To investigate principally the effect of the two-photon coherence, which manifests itself through the last equation of the system (7), we have to simplify the above set of equations by adiabatically eliminating the polarization of the media. In such a case we obtain the following three-equation system [26], where we have supposed that $|E_{1}|^{2}\ll|E_{P}|^{2}$, and where we have neglected the pump transition inversion population with regard to the laser transition inversion population:

$$
\begin{aligned}
&\dot{E}_{1}=-k(E_{1}-D_{1}E_{1}-\sigma C)\ ,\\
&\dot{D}_{1}=-\gamma_{\parallel}(D_{1}E_{1}^{2}+2\sigma E_{1}C+D_{1}-\alpha)\ ,\\
&\dot{C}=-\gamma_{C}(C+E_{1}D_{1})\ ,
\end{aligned}
\tag{8}
$$

where α is the usual pump parameter, C is a new variable defined by $C_{32}=\sigma C$, and where $\gamma_{\parallel}$ and σ are new parameters defined by

$$
\gamma_{\parallel}=\omega_{p}+A_{21},\quad \sigma=\frac{\omega_{p}}{2\gamma_{C}}\ \text{with}\ \gamma_{C}=\gamma_{c}+\frac{\omega_{p}}{2}\ . \tag{9}
$$

Note that a comparison of the numerical results obtained with two numerical simulations using, respectively, the set of equations (7) in which $\gamma_{c}=\gamma_{\perp}$ and the set of equa-

tions (8) shows that the different dynamic behavior in each case is not really different. This is why in the following part of this paper we only study the equation system (8) for which the linear stability analysis is much easier. The equation system (8) describes a laser coherently pumped.

To describe the existence in the fiber of two orthogonal polarization states of the emitted light and to describe their coupling, we must now take into account level (4) and the coupling parameter β of our atomic system (see Fig. 7). Thus as in Sec. III A we have coupled by the electric field and by the population inversion two coherently pumped lasers. A six-equation system is then obtained,

$$\begin{aligned}
\dot{E}_1 &= -k[E_1 - E_1(D_1 + \beta D_2) - \sigma C_1] , \\
\dot{D}_1 &= -\gamma_{\parallel}[D_1(E_1^2 + \beta E_2^2) + 2\sigma E_1 C_1 + D_1 - \alpha] , \\
\dot{C}_1 &= -\gamma_C(C_1 + E_1 D_1) , \\
\dot{E}_2 &= -k[E_2 - E_2(D_2 + \beta D_1) - \sigma C_2] , \\
\dot{D}_2 &= -\gamma_{\parallel}[D_2(E_2^2 + \beta E_1^2) + 2\sigma E_2 C_2 + D_2 - \alpha] , \\
\dot{C}_2 &= -\gamma_C(C_2 + E_2 D_2) .
\end{aligned} \tag{10}$$

The equation system (10) describes a system of two coupled lasers coherently pumped where subscripts 1 and 2 indicate the two orthogonal polarization states of the emitted laser light.

IV. LINEAR STABILITY ANALYSIS OF THE STEADY-STATE SOLUTION

A. Steady-state solution

The linear stability analysis of Eq. (10) can be simplified by introducing the new variable

$$A_+ = A_1 + A_2, \quad A_- = A_1 - A_2 \text{ with } A = \{E, C, D\} .$$

A new six-equation system is then obtained

$$\begin{aligned}
\dot{E}_+ &= -k\left[E_+ - \frac{(E_+ D_+ + E_- D_-)}{2} - \beta\frac{(E_+ D_+ - E_- D_-)}{2} - \sigma C_+\right] , \\
\dot{E}_- &= -k\left[E_- - \frac{(E_- D_+ + E_+ D_-)}{2} - \beta\frac{(E_- D_+ - E_+ D_-)}{2} - \sigma C_-\right] , \\
\dot{C}_+ &= -\gamma_C\left[C_+ + \frac{(E_+ D_+ + E_- D_-)}{2}\right] , \\
\dot{C}_- &= -\gamma_C\left[C_- + \frac{(E_- D_+ + E_+ D_-)}{2}\right] , \\
\dot{D}_+ &= -\gamma_{\parallel}\left[D_+(1+\beta)\frac{(E_+^2 + E_-^2)}{4} + 2D_-(1-\beta)E_+ E_- + \sigma(E_+ C_+ + E_- C_-) + D_+ - 2\alpha\right] , \\
\dot{D}_- &= -\gamma_{\parallel}\left[D_-(1+\beta)\frac{(E_+^2 + E_-^2)}{4} + 2D_+(1-\beta)E_+ E_- + \sigma(E_- C_+ + E_+ C_-) + D_-\right] ,
\end{aligned} \tag{11}$$

with three sets of steady-state solutions: the first is the trivial zero-field solution ($E_{1s}=0, E_{2s}=0$); the second is the monomode solution in which one of the two coupled lasers is above its threshold ($E_{1s}\neq 0, E_{2s}=0$ or $E_{1s}=0, E_{2s}\neq 0$); the third is the bimode solution in which the two coupled lasers are above their threshold ($E_{1s}\neq 0, E_{2s}\neq 0$). In our study we are only interested in this latter solution which can be expressed after calculation as follows:

$$\begin{aligned}
&D_{S_-}=0, \quad C_{S_-}=0, \quad E_{S_-}=0 \\
&D_{S_+} = \frac{2}{1+\beta-\sigma} , \\
&C_{S_+} = -\frac{E_{S_+}}{1+\beta-\sigma} , \\
&E_{S_{+2}} = \frac{4[\alpha(1+\beta-\sigma)-1]}{1+\beta-2\sigma} ,
\end{aligned} \tag{12}$$

where the equality $E_{S_-}=0$ is due to the fact that the two laser subsystems have the same pumping parameter α and therefore have above threshold the same intensity. The last term of Eq. (12) shows the linear dependence of the total intensity ($E_{S_+}^2$) of the laser versus the pump power parameter (α) and allows us to determine the threshold pump power parameter defined by $E_{S_+}^2 = 0$,

$$\alpha_{\text{th}} = \frac{1}{1+\beta-\sigma} . \tag{13}$$

At this point we notice that in our two coupled laser model α is the pumping term of each laser subsystem and is not defined as being the pump parameter of the total laser intensity. This is why for certain sets of parameter conditions, α_{th} can be lower than 1.

B. Instability of the steady-state solution

The linear stability analysis of the system (11) near the steady-state solution (12) leads to a search for the eigenvalue of a 6×6 matrix which reduces to two 3×3 matrices giving the following characteristic polynomials:

$$\lambda^3+\left[\gamma_C+\frac{\gamma_\parallel}{2}+\frac{\gamma_\parallel E_{S_+}^2}{4}-\frac{k\sigma}{1+\beta-\sigma}\right]\lambda^2+\frac{\gamma_\parallel\gamma_C}{2}k(1+\beta-2\sigma)E_{S_+}^2 + \left[\frac{\gamma_\parallel\gamma_C}{2}+\frac{\gamma_\parallel\gamma_C}{4}(1-2\sigma)E_{S_+}^2-\frac{\gamma_\parallel k\sigma}{2(1+\beta-\sigma)}+\frac{\gamma_\parallel k[2(1+\beta)^2-\sigma(3+2\beta)]}{4(1+\beta-\sigma)}E_{S_+}^2\right]\lambda=0\ , \tag{14}$$

$$\lambda^3+\left[\gamma_C+\frac{\gamma_\parallel}{2}+\frac{\gamma_\parallel E_{S_+}^2}{4}-\frac{k\sigma}{1+\beta-\sigma}\right]\lambda^2+\frac{\gamma_\parallel\gamma_C}{2}k\frac{(1-\beta-2\sigma)(1-\beta-\sigma)}{(1+\beta-\sigma)}E_{S_+}^2 + \left[\frac{\gamma_\parallel\gamma_C}{2}+\frac{\gamma_\parallel\gamma_C}{4}(1-2\sigma)E_{S_+}^2-\frac{\gamma_\parallel k\sigma}{2(1+\beta-\sigma)}+\frac{\gamma_\parallel k[2(1-\beta)^2-\sigma(3-2\beta)]}{4(1+\beta-\sigma)}E_{S_+}^2\right]\lambda=0\ . \tag{15}$$

Equation (14) is given by the 3×3 matrix involving the variables E_+, D_+, C_+ while Eq. (15) is given by the 3×3 matrix which involves the variables E_-, D_-, C_-.

From the characteristic polynomial (14), by using the Routh-Hurwitz criteria [26], it is possible to obtain analytically, for the equations involving E_+, D_+, C_+, the Hopf instability conditions and the value of a second threshold α_+ above which no stable stationary solution exists,

$$\alpha_{\text{th}}<\alpha_+ \tag{16}$$

with

$$\alpha_+=\frac{(1+\beta-2\sigma)}{(1+\beta-\sigma)}\left[\frac{\frac{1}{2}\left[\gamma_C-k\frac{\sigma}{(1-\sigma)}\right]^2}{\left[\frac{k^2\sigma[2(1+\beta)^2-\sigma(3+2\beta)]}{(1+\beta-\sigma)^2}-2\sigma\frac{(1+2\beta-\sigma)}{(1+\beta-\sigma)}k\gamma_C-\gamma_C^2(1-2\sigma)\right]}+\frac{1}{(1+\beta-2\sigma)}\right]\ , \tag{17}$$

where we have neglected the decay rate of the population inversion $\gamma_\parallel$ with regard to the other decay rate of our fiber laser.

When the condition $\alpha>\alpha_+$, is realized, the cw steady-state solution ($E_{S_+}^2$) becomes unstable and the total laser intensity (E_+^2) exhibits a self-pulsed working mode in which the intensities of the two laser subsystems (E_1^2 and E_2^2) oscillate in phase at a high frequency which near the Hopf bifurcation is given by

$$\omega_R^2=\frac{E_{S_+}^2\gamma_\parallel\gamma_C k(1+\beta-2\sigma)}{\gamma_C-\frac{k\sigma}{1+\beta-\sigma}}\ . \tag{18}$$

In the same manner, from Eq. (15) it is possible to obtain analytically for the equations involving E_-, D_-, C_-, the Hopf instability condition and the value of a second threshold α_- above which no stable stationary solution exists,

$$\alpha_{\text{th}}<\alpha_- \tag{19}$$

with

$$\alpha_-=\frac{(1+\beta-2\sigma)}{(1+\beta-\sigma)}\left[\frac{\frac{1}{2}\left[\gamma_C-k\frac{\sigma}{(1-\sigma)}\right]^2}{\left[\frac{k^2\sigma[2(1-\beta)^2-\sigma(3-2\beta)]}{(1+\beta-\sigma)^2}-2\sigma\frac{(1-2\beta-\sigma)}{(1+\beta-\sigma)}k\gamma_C-\gamma_C^2(1-2\sigma)\right]}+\frac{1}{(1+\beta-2\sigma)}\right]\ , \tag{20}$$

where we have neglected the decay rate of the population inversion $\gamma_{\parallel}$ with regard to the other decay rate of our fiber laser.

In this case when the condition $\alpha > \alpha_-$, is realized, the cw steady-state solution of our two coupled lasers becomes unstable and the intensities of the two laser system (E_1^2 and E_2^2) produce an opposite phase (antiphase) self-pulsed working mode with a low frequency which near the Hopf bifurcation is given by

$$\omega_L^2 = \frac{E_{S_+}^2 \gamma_{\parallel} \gamma_C k (1-\beta-2\sigma)(1-\beta-\sigma)}{\left[\gamma_C - \frac{k\sigma}{1+\beta-\sigma}\right](1+\beta-\sigma)} . \quad (21)$$

The expressions for the fast frequency (ω_R) and for the low frequency (ω_L) given, respectively, by (18) and (21) are in agreement with the experimental results of Fig. 6. Indeed, as we can observe experimentally ω_R^2 and ω_L^2 depend on ($E_{S_+}^2$) and therefore increase linearly with the pump power and cancel together for the same value of the pump parameter which is the threshold pump power.

The expressions of the instability thresholds given, respectively, by (17) and (20) are rather complicated and their values depend strongly on the relative values of the relaxation constants. Figure 8 shows the α_+ and α_- calculated values versus the ratio k/γ_C for different values of $\sigma = \omega_p / 2\gamma_C$ with $\beta = 0.5$. This figure allows us to suggest that it is possible to obtain in this model threshold instability for a low value of the pump parameter, and that the instability threshold for the fast oscillation mode (α_+) is lower than the instability threshold for the slow one (α_-). Therefore, in our laser, it is possible to obtain pump parameter conditions for the stationary state where only the high-frequency relaxation is undamped and subsists ($\alpha > \alpha_+$) while the lower frequency is damped and disappears ($\alpha < \alpha_-$).

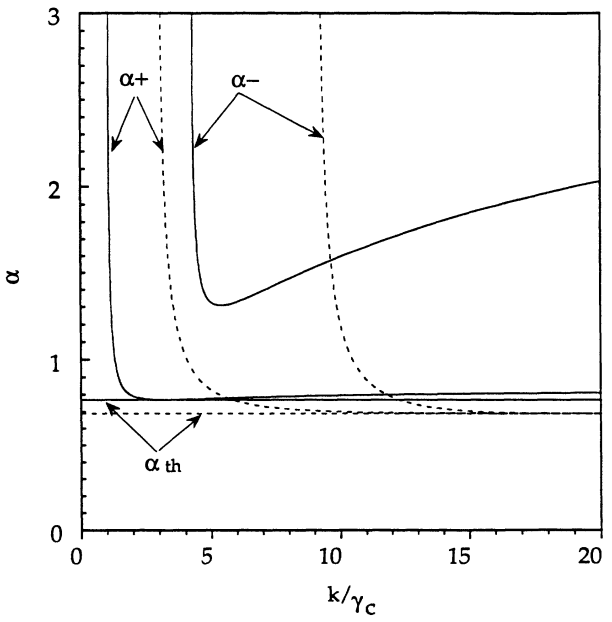

FIG. 8. Instability thresholds α_+ and α_- and pump threshold α_{th} versus k/γ_C for different values of $\sigma = \omega_p / 2\gamma_C$ and with $\beta = 0.5$. The dashed lines correspond to $\sigma = 0.05$ and the solid ones correspond to $\sigma = 0.2$.

V. NUMERICAL SIMULATION

Using a Runge-Kutta method with a variable integration step, we have numerically solved the six coupled differential equations (10) both in the transient and in the stationary regime for the following parameter values:

$$k/\gamma_C = 5, \quad \sigma = 0.05, \quad \beta = 0.5 . \quad (22)$$

With this particular set of parameters, the instability threshold α_- is infinite (see Fig. 8) and we determined that the pump parameter laser threshold is given by $\alpha_{th} = 0.69$ and that the Hopf instability pump parameter for the high frequency is given by $\alpha_+ = 0.96$.

For the pumping condition $\alpha_{th} < \alpha < \alpha_+ < \alpha_-$, the transient dynamics numerically obtained are represented in Fig. 9, where the responses of the intensities of the two coupled lasers are given, respectively, by the upper and the middle traces [Figs. 9(a) and 9(b)] while the time variation of the total intensity is given on the lower trace. These figures are qualitatively in good agreement with those of Fig. 3 describing the observed dynamics of the two orthogonal states of the fiber laser. Indeed, the two coupled lasers show transient behavior that is a superposition of two damped oscillation modes which present beating, and due to the antiphase phenomena, the total intensity shows only the high-frequency damped oscillations [Fig. 9(c)].

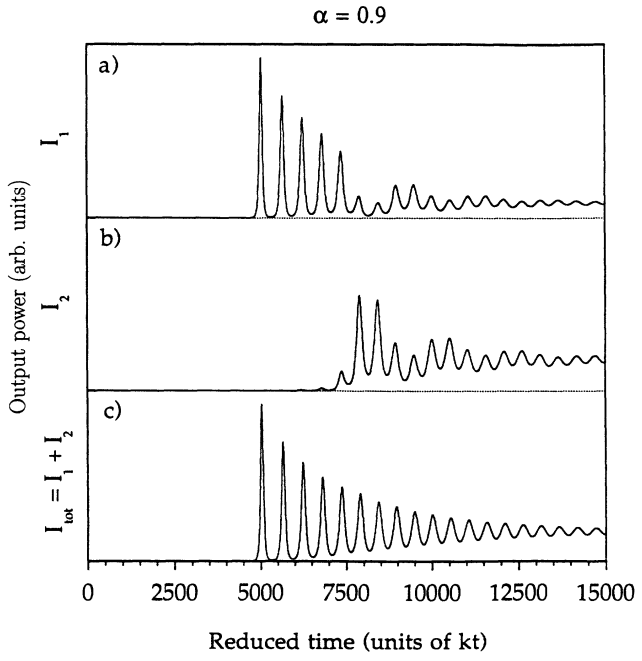

FIG. 9. Numerical simulation of the transient behaviors of the intensities I_1 and I_2 and of the total intensity I_{tot} of the two coupled lasers coherently pumped when $\alpha_{th} < \alpha < \alpha_+ < \alpha_-$, and with the following parameters: $\alpha = 0.9$, $\gamma_{\parallel}/k = 3.10^{-4}$, $k/\gamma_c = 5$, $\sigma = 0.05$, $\beta = 0.5$.

By increasing the pump parameter to a value of $\alpha=1.22$, leading to $\alpha_+<\alpha<\alpha_-$, the laser delivers in the stationary state, for the total intensity, an infinite train of pulses [Fig. 10(c)]. As previously, in the transient behavior, the two orthogonal polarization states present beating and antiphase phenomena. In this case, however, only the lower frequency is damped while the higher one subsists in the steady state [Figs. 10(a) and 10(b)]. These numerical results are qualitatively in good agreement with the experimental results of Fig. 4.

In contrast with the experiment, nothing limits numerically the value of the pump parameter. Figures 11–13 show interesting new types of dynamic behavior for higher values of the pump parameter. For example, for $\alpha=1.35$, the system shows a $2T$ periodic phenomena for the two polarization states [Figs. 11(a) and 11(b)], while for the total intensity, due to the antiphase phenomena, the system shows only a single T periodic oscillation. By increasing the pump parameter to a higher value ($\alpha=1.47$), the system presents more complex dynamics. A $4T$ periodic oscillation appears for the two polarization states [Figs. 12(a) and (b)], and a $2T$ for the total intensity [Fig. 12(c)]. For higher values of the pump parameter, the oscillations of the two polarizations lose all regularity and show chaotic behavior [Figs. 13(a) and 13(b)]. Due to the antiphase phenomena, the amplitude variation of each pulse is less important for the total intensity than for those of the two states of polarization [Fig. 13(c)].

A more detailed study of Eqs. (16) and (17) indicates that the instability threshold α_+ involving the variables E_+, D_+, C_+ exists only if the condition $\alpha_{\text{th}}<\alpha_+$ is verified, i.e., only if laser parameters satisfying the following inequalities:

$$\sigma<\tfrac{1}{2},\quad \frac{\gamma_C}{k}<\frac{\{[3(1-\sigma)\sqrt{2\sigma}-2\sigma(2-\sigma)]\}}{(1-2\sigma)(3-2\sigma)}\ , \tag{23}$$

where we have fixed $\beta=0.5$; note that $\sigma=\omega_p/2\gamma_C$ with γ_C the loss rate of the two-photon coherence and ω_p the absorption probability of a pump photon. A more de-

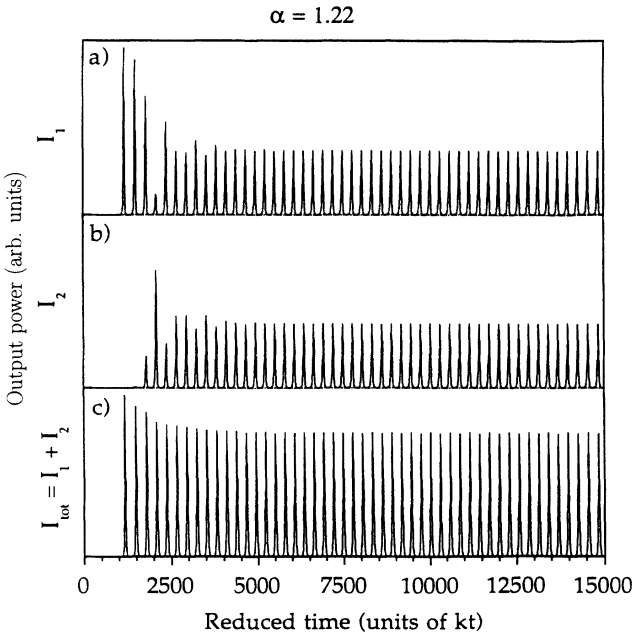

FIG. 10. Numerical simulation of the transient behaviors of the intensities I_1 and I_2 and of the total intensity I_{tot} of the two coupled lasers coherently pumped when $\alpha_+<\alpha<\alpha_-$, and with the following parameters: $\alpha=1.22$, $\gamma_\parallel/k=3.10^{-4}$, $k/\gamma_c=5$, $\sigma=0.05$, $\beta=0.5$.

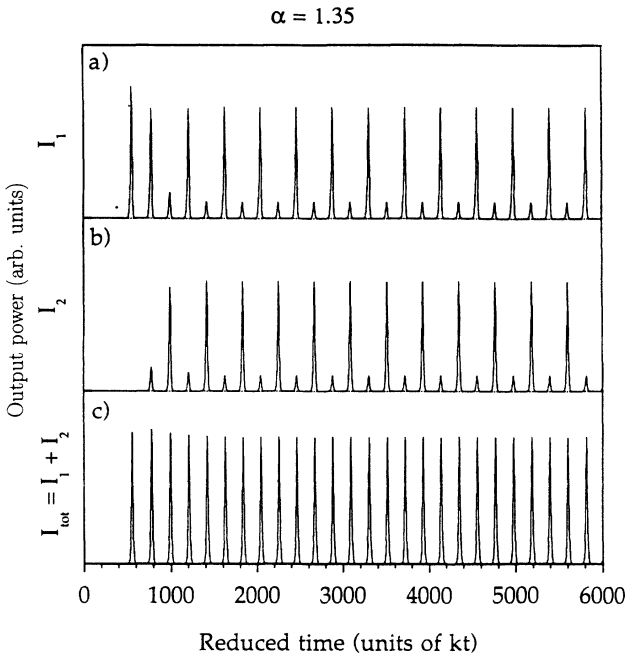

FIG. 11. Same as Fig. 10, but with a pump parameter $\alpha=1.35$.

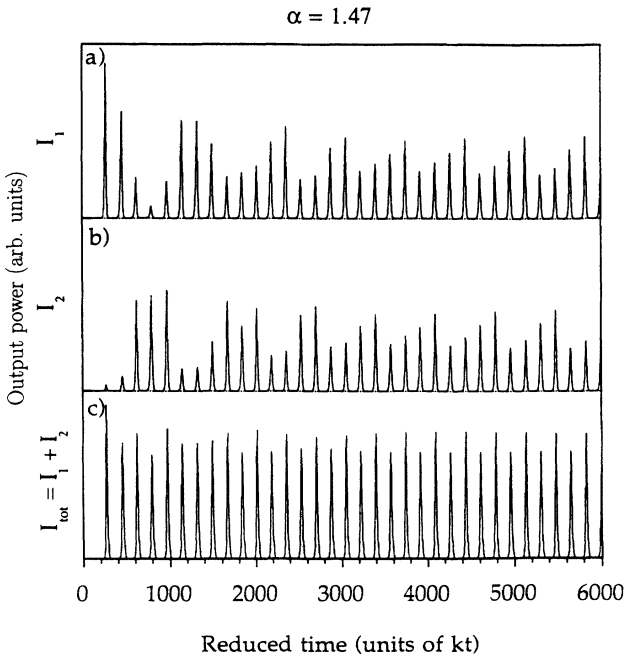

FIG. 12. Same as Fig. 10, but with a pump parameter $\alpha=1.47$.

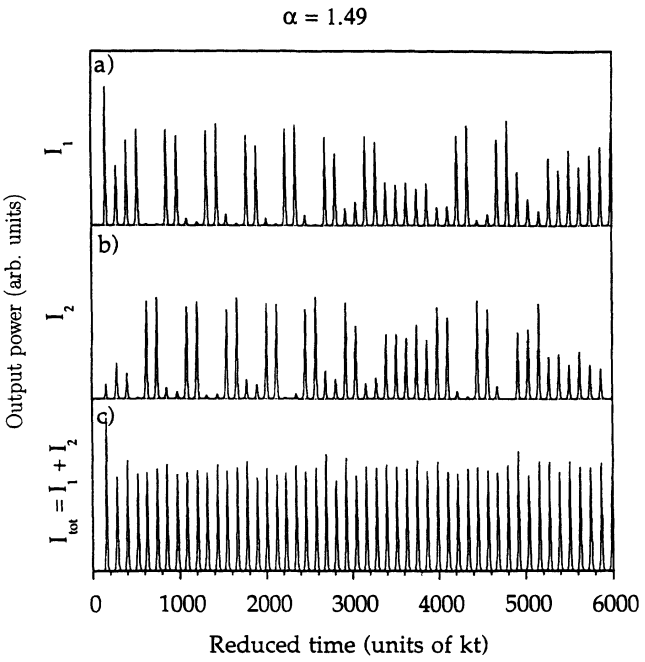

FIG. 13. Same as Fig. 10, but with a pump parameter $\alpha = 1.49$.

tailed study of the instability conditions (19) and (20) involving the variables E_-, D_-, C_- gives approximately the same inequalities.

In a solid-state laser and in particular in the fiber laser, the first part of the inequality [Eq. (23)] is always valid. Conversely, the second one, which requires that γ_c must be lower or of the same order of magnitude as the laser-field loss-rate parameter (k), seems to be more difficult to realize due to the fact that in a fiber laser the value of the parameter γ_c is generally between 3 and 5 orders of magnitude higher than the value of k.

At this point, in order to allow this mathematical model, which allows a very good description of all the results obtained experimentally, to be applied to the case of the doped fiber laser, we assume another possible physical interpretation of the variable C.

The hypothesis is that the second part of the inequality in Eq. (23) can be verified in a doped fiber laser if we understand now the variable C as a loss term rather than a coherence term. Indeed, a more detailed study of the equation system (8), and more particularly of its third equation, shows that the variable C varies like the opposite of the stimulated emission gain. By inserting $C = -E_1 D_1$ in the first equation of the system (8) we obtain a term $-k\sigma E_1 D_1$ describing a new "absorption" loss term taking place inside the doped fiber. The physical origin of this loss can be explained by the fact that doped fibers are a long inhomogeneous amplifying medium pumped longitudinally, and therefore, some part of the active medium can be amplifying while another one is absorbing. In our equation system [Eq. (8)] the additional loss term $-k\sigma E_1 D_1$ does not act instantaneously in the equation describing the time evolution of the electric field [i.e., the first equation of Eq. (8)] but rather acts with a time delay (i.e., a dephasing) depending on the relative value of the relaxation constant γ_C and k. In our hypothesis of losses due to the inhomogeneity of gain along the active medium this time delay is linked to a propagation time inside the doped fiber. Under this condition the relaxation parameter (γ_C) can be of the same order of magnitude as the laser-field loss-rate parameter (k), and therefore, the two inequalities of Eq. (23) can now be verified for a doped fiber laser.

In conclusion, in order to describe the dynamics of the fiber laser, we have studied a semiclassical model of two coupled lasers coherently pumped. This model exhibits various interesting modes of behavior and allows a good description of the different types of dynamic behavior experimentally observed, but for the mathematical model to be applied to the case of a fiber laser we must interpret the newly introduced variable of our laser model as describing losses permitting one to take into account the z dependence of the gain inside the fiber. This discussion suggests that for further investigations of fiber lasers we must take into account dynamics of the propagation phenomena and therefore use partial differential equations.

ACKNOWLEDGMENTS

The authors wish to thank Pierre Glorieux, Serge Bielawski, and Dominique Derozier for stimulating discussions and Michel Monerie (CNET Lannion) for providing the doped fibers. The Laboratoire de Spectrométrie Physique is "associé au CNRS."

[1] H. Haken, Phys. Lett. **53**, 77 (1975).
[2] F. T. Arecchi and R. G. Harrison, *Instabilities and Chaos in Quantum Optics* (Springer-Verlag, Berlin, 1987).
[3] N. B. Abraham, L. A. Lugiato, and L. M. Narducci, J. Opt. Soc. Am. **2**, 7 (1985) and references therein.
[4] R. Graham, Phys. Lett. **58**, 440 (1976).
[5] P. A. Khandokin, Ya. I. Khanim, and I. V. Koriukin, Opt. Commun. **62**, 307 (1983).
[6] W. Forysiak, R. G. Harrisson, and J. V. Moloney, Phys. Rev. A **39**, 54 (1985).
[7] C. O. Weiss, J. Brock, Phys. Rev. Lett. **57**, 2804 (1986).
[8] D. Dangoisse, P. Glorieux, and D. Hennequin, Phys. Rev. A **36**, 4775 (1987).
[9] M. F. Tarroja, A. Sicam, L. W. Casperson, and P. Chencosol, Opt. Commun. **84**, 162 (1991).
[10] E. Lacot, F. Stoeckel, and M. Chenevier (unpublished).
[11] S. Bielawski, D. Derozier, P. Glorieux, Opt. Commun. **83**, 97 (1991).
[12] S. Bielawski, D. Derozier, and P. Glorieux, Phys. Rev. A **46**, 2811 (1992).
[13] R. Collins, D. Nelson, A. Schawlow, W. Bond, C. G. B. Garret, and W. Kaiser, Phys. Rev. Lett. **5**, 303 (1960).
[14] H. Risken and K. Numendal, J. Appl. Phys. **39**, 4662 (1968).

[15] J. A. Fleck, R. E. Kidder, J. Appl. Phys. **36**, 2327 (1965).
[16] L. W. Casperson, Phys. Rev. A **21**, 911 (1975).
[17] M. L. Shih, P. W. Milonni, and J. R. Ackerhalt, J. Opt. Soc. Am. B **2**, 130 (1985) and references therein.
[18] G. P. Puccionni, M. V. Tratnik, J. E. Sipe, and G. L. Oppo, Opt. Lett. **12**, 242 (1987).
[19] J. C. Ryan, N. M. Lawandy, Opt. Commun. **64**, 54 (1987).
[20] F. Sanchez, P. Le Boudec, P. L. Francois, and G. Stephan, Phys. Rev. A **48**, 2220 (1993).
[21] K. Otsuka, P. Mandel, S. Bielawski, D. Derozier, and P. Glorieux, Phys. Rev. A **46**, 1692 (1992).
[22] P. Mandel, M. Georgiou, K. Otsuka, and D. Pieroux, Opt. Commun. **100**, 341 (1993).
[23] K. Otsuka, M. Georgiou, and P. Mandel, Jpn. J. Appl. Phys. **31**, L1250 (1992).
[24] K. Otsuka, P. Mandel, M. Georgiou, and C. Etric, Jpn. J. Appl. Phys. **32**, L318 (1993).
[25] P. Berge, Y. Pomeau, and C. Vidal, *L'Ordre dans le Chaos* (Hermann, Paris, 1986).
[26] E. Lacot, Ph.D. thesis, University J. Fourier, Grenoble, France, 1992 (unpublished).
[27] H. Statz and C. L. Tang, J. Appl. Phys. **35**, 1377 (1964).
[28] C. L. Tang, H. Statz, and G. De Mars, J. Appl. Phys. **34**, 2289 (1963).
[29] H. Haken, *Laser Theory* (Springer-Verlag, Berlin, 1984).
[30] H. Haken, Z. Phys. **190**, 327 (1966).
[31] H. Risken, C. Schmid, and W. Weidlich, Z. Phys. **194**, 337 (1966).
[32] L.W. Casperson, Phys. Rev. A **21**, 911 (1980).